FULL PAPER

Inverted Layer-By-Layer Fabrication of an Ultraflexible and Transparent Ag Nanowire/Conductive Polymer Composite Electrode for Use in High-Performance Organic Solar Cells

Youngmin Kim, Tae In Ryu, Ki-Hoon Ok, Min-Gi Kwak, Sungmin Park, Nam-Gyu Park, Chul Jong Han, Bong Soo Kim, Min Jae Ko, Hae Jung Son, and Jong-Woong Kim**

A highly flexible and transparent conductive electrode based on consecutively stacked layers of conductive polymer (CP) and silver nanowires (AgNWs) fully embedded in a colorless polyimide (cPI) is achieved by utilizing an inverted layer-by-layer processing method. This CP-AgNW composite electrode exhibits a high transparency of >92% at wavelengths of 450–700 nm and a low resistivity of 7.7 Ω $\square^{-1}$, while its ultrasmooth surface provides a large contact area for conductive pathways. Furthermore, it demonstrates an unprecedentedly high flexibility and good mechanical durability during both outward and inward bending to a radius of 40 μm. Subsequent application of this composite electrode in organic solar cells achieves power conversion efficiencies as high as 7.42%, which represents a significant improvement over simply embedding AgNWs in cPI. This is attributed to a reduction in bimolecular recombination and an increased charge collection efficiency, resulting in performance comparable to that of indium tin oxide-based devices. More importantly, the high mechanical stability means that only a very slight reduction in efficiency is observed with bending (<5%) to a radius of 40 μm. This newly developed composite electrode is therefore expected to be directly applicable to a wide range of high-performance, low-cost flexible electronic devices.

1. Introduction

Transparent and conductive materials are an important component in optoelectronic devices such as touch screens, organic light emitting diodes, and organic solar cells, but the inherent brittleness and high cost of commonly used metal oxides such as indium tin oxide (ITO) have so far greatly limited their practical application.[1] There is therefore a need for a more cost-effective and flexible alternative to ITO that can provide excellent transparency, low sheet resistance, and sufficient mechanical stability when used in optoelectronic devices. This has led to active interest in materials such as alternative amorphous metal oxides,[2] conductive polymers,[3] graphene,[4] carbon nanotubes,[5] and metal nanomaterials.[6]

Of the various alternatives to ITO, silver nanowires (AgNWs) have emerged as the most promising candidate by virtue of their porous network structure.[6e–9] They also offer the advantage of being easily formed into a highly flexible and transparent conductive film through a simple and readily scalable solution processing method of spin coating, deep coating, and air spraying a AgNW dispersion. Yet despite the success that has been achieved in incorporating AgNWs into optoelectronic devices, there are still a number of critical issues holding back their practical use. For example, in organic solar cells, the rough surface of the AgNW network presents a problem when used as a substitute for an ITO bottom electrode as it can easily penetrate the soft organic layer and short circuit the device.[8] Furthermore, the limited contact between the AgNWs

Dr. Y. Kim, K.-H. Ok, M.-G. Kwak, Dr. J.-W. Kim
Display Components & Materials Research Center
Korea Electronics Technology Institute
Seongnam 463-816, South Korea
E-mail: wyjd@keti.re.kr; wyjd78@gmail.com
T. I. Ryu, Prof. N.-G. Park
School of Chemical Engineering
Sungkyunkwan University
Suwon 440-746, South Korea
S. Park, Prof. B. S. Kim,
Dr. M. J. Ko, Dr. H. J. Son
Photoelectronic Hybrid Research Center
Korea Institute of Science and Technology
Seoul 136-791, South Korea
E-mail: hjson@kist.re.kr
S. Park
Department of Chemistry
Korea University
Seoul 136-713, South Korea
Dr. C. J. Han
Display Convergence Research Center
Korea Electronics Technology Institute
Seongnam 463-816, South Korea
Prof. B. S. Kim
Department of Science Education
Ewha Womans University
Seoul 120-750, South Korea

DOI: 10.1002/adfm.201501046

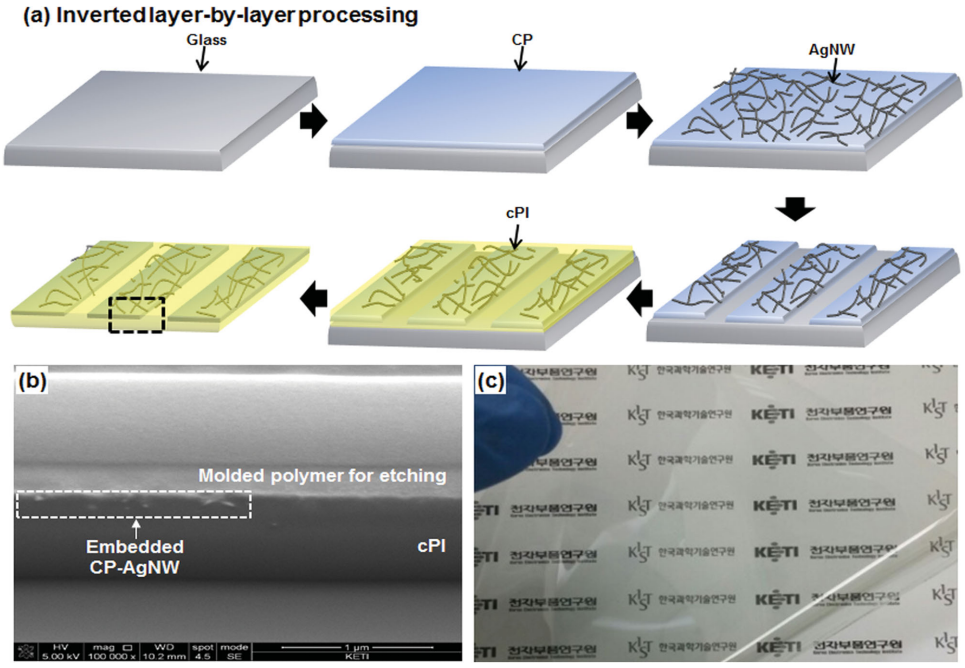

Figure 1. a) Schematic diagram showing the various stages in the inverted layer-by-layer process. b) Cross-sectional SEM image of a patterned CP-AgNW composite electrode embedded in a cPI film. c) Photograph showing the transparency of the fabricated film.

and upper interlayer is detrimental to effective charge collection.[9] Possible solutions include creating a planar AgNW surface by coating onto a polymer film and pressing with a glass plate or silicon rubber, but the very high force required tends to make such lamination impractical.[8b] Others have attempted to create an AgNW hybrid with conductive polymers or metal oxides,[10] which in most cases is successful in creating a smooth coating of conductive material on the AgNW network that reduces the surface roughness from 50 nm to a root mean square (R_{RMS}) of about 5 nm. However, in order to ensure complete planarization, a thick layer is required over the whole AgNW network that invariably results in an increased series resistance and reduced transparency. Alternatively, a smooth conductive AgNW surface can be achieved by coating a transparent liquid polymer onto a precoated AgNW network, followed by the drying and peeling of this film from a supporting substrate.[8a,c,9] Electrodes produced in this manner tend to have a very smooth surface, resulting in an extremely low leakage current when used in an organic electronic device, but as the AgNWs are buried inside the polymer matrix only a very small area is exposed at the surface. This results in a very limited conductive pathway, and consequently the charge injection into the active layer of an organic light emitting diode (OLED) is poor. It is therefore of great importance to develop a reliable fabrication method for highly flexible and conductive electrodes that can simultaneously satisfy the requirements for surface smoothness and a large surface coverage area.

In this study, we developed a highly flexible composite electrode based on embedding a AgNW network and conductive polymer (CP) layer in a colorless polyimide (cPI) matrix, with the intent to create both high transparency and low electrical resistivity. This structure was achieved by using an inverted layer-by-layer method, in which alternating layers of CP and AgNW were stacked to produce a highly smooth surface with a large surface coverage of conductive pathways. This material was subsequently applied as the bottom electrode in a polymer solar cell, and its effect on the power conversion efficiency under various bending conditions is herein discussed.

2. Results and Discussion

Figure 1a schematically illustrates the inverted layer-by-layer fabrication process used to create electrodes consisting of a CP-AgNW composite embedded in a cPI matrix (CP-AgNWs/cPI). Neutral poly(3,4-ethylenedioxythiophene):polystyrene sulfonate (PEDOT:PSS) was chosen as the CP component on the basis of its high electrical conductivity and processability, not to mention the fact that its flexibility, low-cost production, and ready availability on a large scale provides a significant advantage insofar as industrial application is concerned.[3b] In the first stage of this process, a solution of neutral PEDOT:PSS containing a binding material was spin-coated onto cleaned glass, with the resulting film then being annealed at 120 °C for 30 min. A specially designed epoxy-based binder in the film serves to increase the films resistance to dispersion of the PEDOT:PSS particles in water, while also making it soluble in an acidic liquid. A dispersion of AgNWs in alcohol was then deposited onto the PEDOT:PSS film and carefully dried under infrared illumination for 10 min. A mature photolithography technique was used for the highly selective and reproducible micropatterning of the composite electrode,[11] wherein a stacked PEDOT:PSS and AgNW composite on a glass substrate was soaked in a dilute acid. As shown in Figure S1 (Supporting Information), this created a very ordered pattern with high, sharp edges; and despite the very different chemical properties of the two components,

a resolution finer than 30 μm was possible without any significant defects. Onto this patterned AgNW-PEDOT:PSS composite electrode, a cPI varnish layer was applied by spin-coating, and then thermally treated at 200 °C for 1 h. The cPI employed in this study was highly transparent and colorless, yet still exhibits suitable mechanical properties (6 GPa of Young's modulus and 300 MPa of tensile strength). Furthermore, according to the manufacturer, it is capable of withstanding 5 suns of illumination and absorbs less than 1% of water, both of which make it ideal for use in flexible organic solar cells (OSCs). The developed CP-AgNWs/cPI electrode also showed high durability from various organic solvent treatments. As shown in Figures S2 and S3 (Supporting Information), it did not exhibit any damage even after keeping the solvent drop on the electrode surface for 10 min, suggesting its wide applicability to wet-process-based electronic devices. The film thickness was controlled by varying the spinning velocity, which was controlled so as to provide an optimal balance between flexibility and reliability. Finally, the sample was soaked in water to allow the film created to be safely peeled off the supporting glass substrate, a process which was aided by the hygroscopic swelling of the PEDOT:PSS layer and cPI film.

The field-emission scanning electron microscope (FESEM) image in Figure 1b shows the cross-section of a patterned CP-AgNWs electrode embedded in cPI and completely buried beneath a smooth and planar molded polymer suitable for etching. This indicates that it is not in fact necessary to form a thick interlayer on CP-AgNW/cPI in order to planarize the AgNW network and reduce their high peak-to-valley roughness (R_{PV}). **Figure 2**b shows the surface morphology of the AgNW network created on the CP film (AgNW-CP) during the second and third stages of fabrication in Figure 1, with the well dispersed nature of these NWs and their perfect contact with the CP layer suggesting a large interfacial area between the two. This large contact area should provide abundant conduction pathways, which is known to be favorable for charge injection from the electrode to the active layer of the device (or charge collection in the opposite direction).[9] It is also worth noting that the CP-AgNW/cPI electrode obtained after the final step (Figure 2c) exhibits a more continuous and uniform surface morphology than even a spin-coated CP film on glass (Figure 2a).

Atomic force microscopy (AFM) measurement of the surface roughness of the films was consistent with the SEM results: the CP-AgNW/cPI in Figure 2f exhibiting a small RMS and R_{pv} values of 2.0 and 26.2 nm, respectively, which represents a significant decrease from the 30.1 nm RMS and 228.7 nm R_{pv} of the AgNW-CP film in Figure 2e. Such low RMS value is similar to that of sputter-derived commercial ITOs used in our studies (RMS roughness = 2.5 nm). This reduction can be attributed to the processing method used, in that CP-AgNW/cPI was originally formed on a smooth glass surface. Moreover, some of the agglomerated CP particles evident in Figure 2a are no longer observed in Figure 2c. For comparison, an electrode was also prepared from stacked layers of CP and AgNWs, but overcoated in a 50 nm thick PEDOT:PSS film to provide surface planarization of the AgNW network. As shown in Figure 2h, this electrode had a much higher surface roughness, with a R_{pv} of 186.2 nm and a RMS of 16.6 nm. What is more, even a 100 nm thick PEDOT:PSS overlayer (Figure 2i) failed to provide any significant improvement in film roughness. On the basis of this, the newly developed fabrication method is considered a very effective means of obtaining CP-AgNW composite electrodes with a high surface uniformity and planarity. More importantly, the simplicity of this process allows for the fabrication

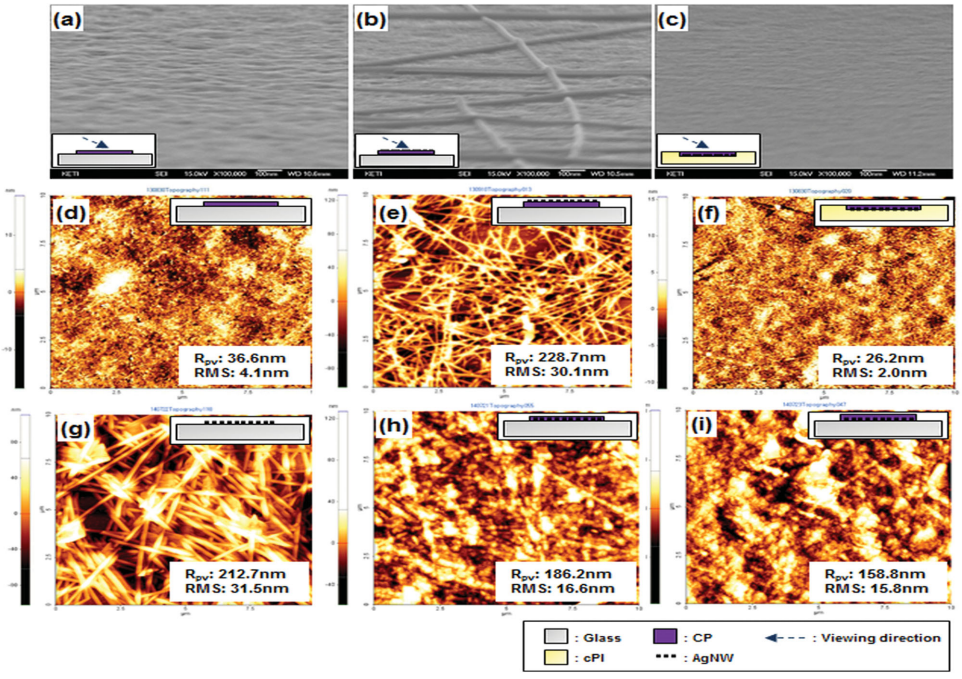

Figure 2. a–c) Tilted SEM and d–i) AFM images showing the surface of different composite electrodes. a) PEDOT:PSS (50 nm)/glass, b) AgNW/PEDOT:PSS (50 nm)/glass, c) PEDOT:PSS (50 nm)/AgNW embedded in cPI, d) PEDOT:PSS (50 nm)/glass, e) AgNW/PEDOT:PSS (50 nm)/glass, f) PEDOT:PSS (50 nm)/AgNW embedded in cPI, g) AgNW/glass, h) PEDOT:PSS (50 nm)/AgNW/glass, i) PEDOT:PSS(100 nm)/AgNW/glass.

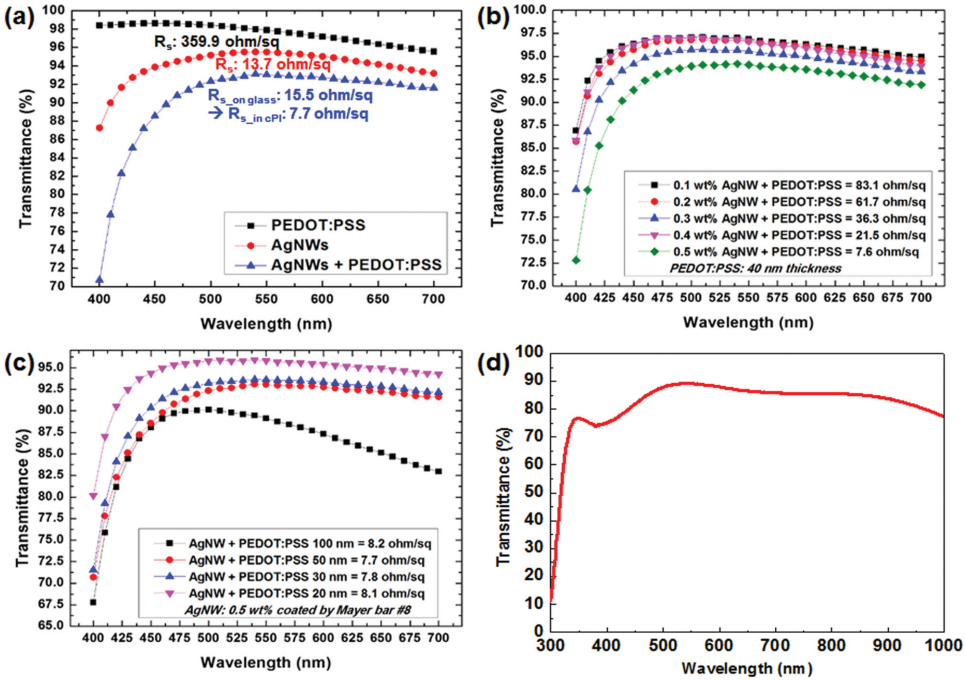

Figure 3. Measured transmittance and corresponding sheet resistance relative to cPI for various: a) electrode structures, b) AgNW nanowire inks, and c) PEDOT:PSS layer thicknesses. d) Transmittance of ITO glass.

of ultrasmooth and flexible transparent electrodes over a large area of at least up to 180 × 220 mm^2, as shown in Figure S4 (Supporting Information). Furthermore, the size of the film can easily be made even larger by employing a roll-to-roll based polymer coating apparatus such as a slot-die or microgravure coating system.

Figure 3a shows the visible wavelength transmittance of various electrodes, not including any reduction in transmittance by the cPI substrate. Note that even over a very broad spectral range of 450–700 nm all of the films tested exhibit a high transmittance of more than 90%, and the sheet resistance (R_s) of the AgNW-PEDOT:PSS film (15.5 Ω h^{-1}) is comparable to that of a AgNW network alone (13.7 Ω h^{-1}) when a glass substrate is used. Notably, however, the R_s of the CP-AgNW/cPI film is dramatically reduced to 7.7 Ω h^{-1}, which is due mainly to the decrease in contact resistance between the AgNWs that is created by the removal of residual polyvinylpyrrolidone (PVP) and shrinkage of the cPI during curing at 200 °C. This combination of excellent conductivity and transmittance would make such an electrode ideally suited for application in high-performance organic electronic devices.

The effect of increasing the density of AgNWs can be seen in Figure 3b, in that there is a significant decrease in R_s as the concentration of the AgNW dispersion is increased from 0.1 to 0.5 wt%; however, this is accompanied by only a very small 5% reduction in transmittance. Thus, the film prepared from a 0.5 wt% solution has a transmittance of 92%–94% in the 450–700 nm frequency range, and a R_s of 7.6 Ω □$^{-1}$. Following optimization of the PEDOT:PSS thickness in Figure 3c, this transmittance was improved to 93%–96% in the same range, while still maintaining a similar conductivity (R_s = 8.1 Ω □$^{-1}$). This implies that the lateral conductance of the composite film is predominantly determined by the AgNW density rather than the thickness of the PEDOT:PSS layer. On the basis of this, further optimization of the processing conditions was able to achieve an extremely uniform (RMS = 2.0 nm) film with a transmittance of over 92% at 450–700 nm and a R_s of 7.6 Ω □$^{-1}$ properties. The transmittances are comparable to those of sputtered crystalline ITO as shown in Figure 3d and rather, the sheet resistance is lower than 15 Ω □$^{-1}$ of the ITO glass.

To test the mechanical durability of the film, it was subjected to bending to various curvatures ranging from 160 to 40 μm, as illustrated in Figures S6 and S7 (Supporting Information). **Figure 4**a shows the change in resistance in response to outward (tensile stress) or inward (compressive stress) bending as a function of the bending radius; the change in resistance being expressed as $(R - R_o)/R_o$, where R is the resistance after bending and R_o is the initial resistance. Note that the applied strain is equal to the thickness of the film divided by two-times the bending radius. It is evident from this that the film is highly flexible and has a high mechanical stability; but more importantly, there is almost no increase in resistance after bending to a radius of 100–160 μm. Indeed, even with a 40 μm bending radius that corresponds to a strain of 25% (film thickness: 20 μm), the resistance only increased by 5% for inward bending and <10% for outward bending. We also fabricated a buckled structure of the CP-AgNW/cPI electrode in a thickness of 5 μm to measure the smallest curvatures that can be formed by a preparation method illustrated in Figure S9 (Supporting Information). Figure 4b shows an example of the fabricated buckles on the composite electrode, and we measured the resistance of the electrodes before and after the buckle formation. This measurement shows that the resistance increased

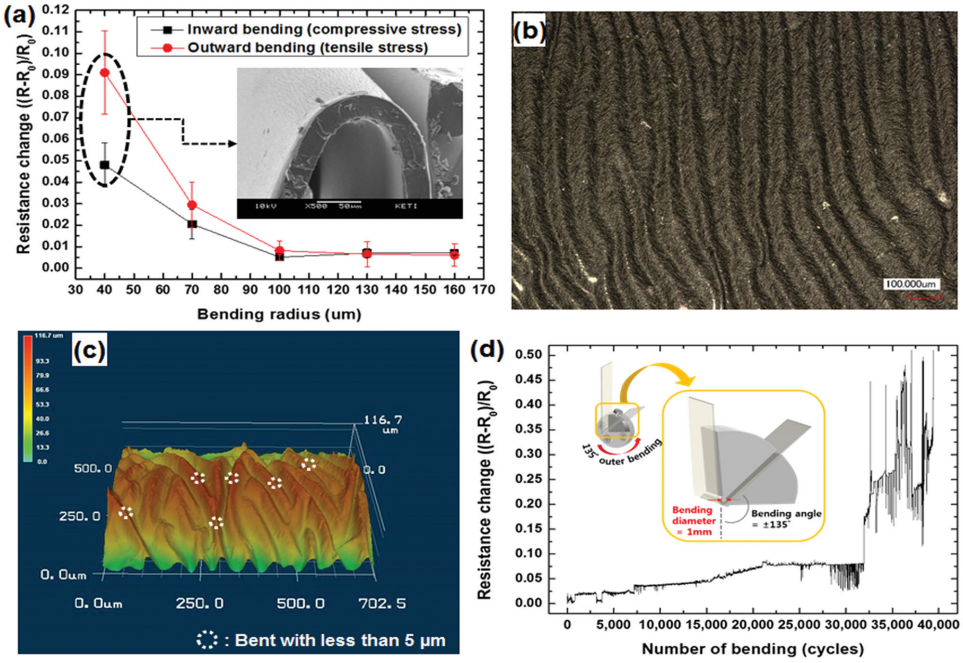

Figure 4. Bending reliability of the fabricated films: a) effect of bending radius on the resistance of a 20 μm thick film, b) fabricated buckles of 5 μm thick film, c) 3D surface profile of the buckled structure, d) change in resistance with repeated bending to a radius of 500 μm (film thickness: 20 μm).

within 10% even after the formation of such buckles, in comparison with that of an as-fabricated one. At this point, we should note that the radius of the buckle curvatures was ranged from 3 to 20 μm as represented in Figure 4c, which means that the fabricated electrodes could withstand a real folding stresses with a good stability. This flexibility and foldability could also be found in the Movie S1 (Supporting Information). To the best of our knowledge, this is the smallest bending curvature that has been reported for such a material, and so it was subsequently subjected to long-term cyclic (1 Hz) bending testing to an inward and outward radius of 500 μm (see Figures S10 and S11, Supporting Information). This found that the film has excellent bending fatigue strength, with Figure 4d showing that its resistance increased by less than 5% after 10 000 cycles, and even after 30 000 cycles there was still no dramatic increase in resistance. This high mechanical flexibility originates from the unique structure of the CP-AgNW/cPI electrode, in that fully embedding the composite electrode underneath the surface of cPI creates an enlarged interfacial area between the electrode and cPI. Exceptionally good adhesion of cPI to the CP and AgNWs also contributed to this high mechanical stability.

In order to evaluate the performance of the CP-AgNW/cPI electrode, it was used in the fabrication of a bulk heterojunction OSCs with a device configuration of cPI/CP-AgNW/hole transporting material/active layer/TiO_2/Al (**Figure 5**). The active layer of this device was a ≈100 nm thick bulk heterojunction composed of poly({4,8-bis[(2-ethylhexyl)oxy]benzo[1,2-b:4,5-b′]dithiophene-2,6-diyl}{3-fluoro-2-[(2-ethylhexyl)carbonyl]thieno[3,4-b]thiophenediyl}) (P1, Figure 5) and [6,6]-phenyl-C71-butyric acid methyl ester ($PC_{71}BM$) in a 1:1.5 ratio by weight. A schematic of the device architecture is shown in Figure 5a, and a SEM image showing the device in cross-section is given in Figure 5b. Note that all layers exhibit very smooth interfaces and are parallel to each other without abruption, with the lack of any discernible artifacts from shunting or surface recombination being beneficial to the performance of the device. To provide a comparison, solar cell devices were also produced by replacing the CP-AgNW/cPI electrode with a AgNW/cPI electrode prepared though a simple AgNW embedding method, details of which are provided in Figure S12 (Supporting Information). The photovoltaic performance of these two solar cell devices under a simulated AM 1.5G 0.888 sun illumination (88.8 mW cm^{-2}) is represented by the current density–voltage (J–V) curves in **Figure 6**a and the characteristic solar cell data summarized in **Table 1**. We can see from this that the CP-AgNW/cPI electrode produces the best efficiency of 6.81%, with a short-circuit current (J_{sc}) of 13.61 mA cm^{-2}, a fill factor (FF) of 0.60, and an open-circuit voltage (V_{oc}) of 0.740. From an average of ten such devices, the power conversion efficiency (PCE) was determined to be 6.75%, with a J_{sc} (Ave.) of 13.71 mA cm^{-2}, a FF (Ave.) of 0.592, and a V_{oc} (Ave.) of 0.739. By contrast, the parameters of the control AgNW/cPI-based device were all notably lower, with a J_{sc} of 12.82 mA cm^{-2}, a FF of 0.393, and a V_{oc} of 0.742 resulting in a PCE of 4.21%. The superior performance of CP-AgNW/cPI-based device is considered most likely due to its greater number of conductive pathways for charge collection on the electrode surface. The series resistance of each solar cell device was subsequently calculated from the slope of their respective I–V curve, revealing the CP-AgNW/cPI-based device to have a series resistance (R_s) of 11.0 Ω cm^2 that is substantially lower than the 28.7 Ω cm^2 of the AgNW/cPI-based device, and comparable to that of ITO-based devices (8.5 Ω cm^2). This suggests that the reduced contact resistance between the electrode and the hole injection layer plays an important role in increasing the charge collection efficiency and PCE of the device, and could also explain the observed increase in FF.

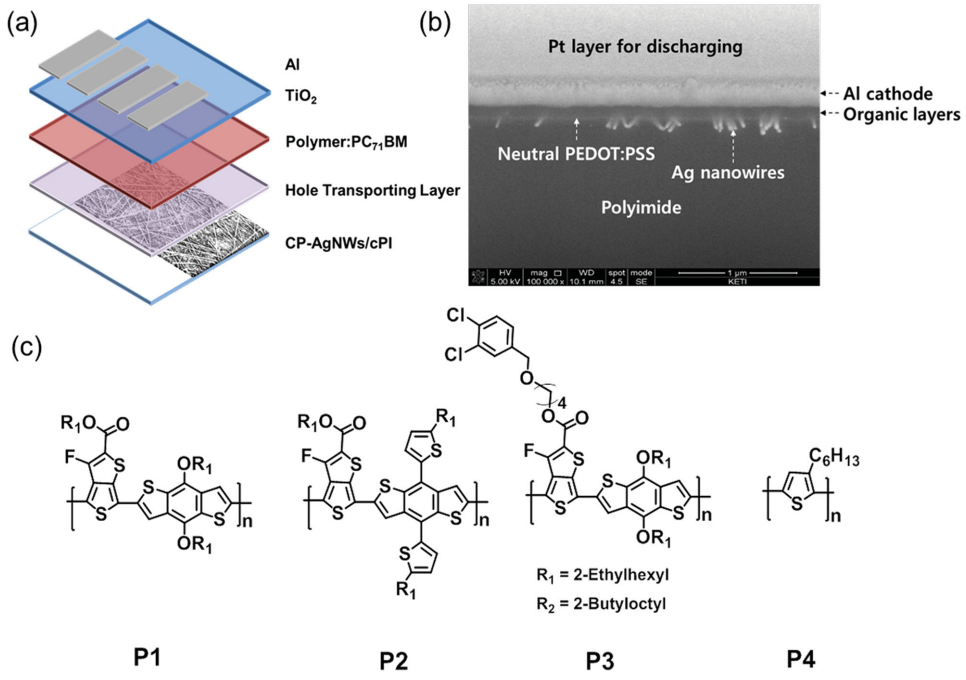

Figure 5. a) Structure of an organic solar cell device based on a CP-AgNW/cPI electrode, b) cross-sectional view of the organic solar cell device, c) chemical structures of the polymers.

The parallel resistances (R_p) of the devices are determined to be 4.16, 1.04, and 5.13 K Ω cm^2 for CP-AgNW/cPI, AgNW/cPI, and ITO based solar cells, respectively. Figure S13 (Supporting Information) shows dark *J*–*V* curves of the P1 solar cell devices and their reverse saturation currents (J_o) were determined from the curves. The solar cell devices made from CP-AgNW/cPI and ITO exhibited very low J_os of 4.4×10^{-7} and 2.6×10^{-7} A, respectively, while the device with AgNW-cPI showed relatively high J_o value of 1.4×10^{-6} A. This result suggests much reduced leak current of the CP-AgNW/cPI-based solar cell device compared

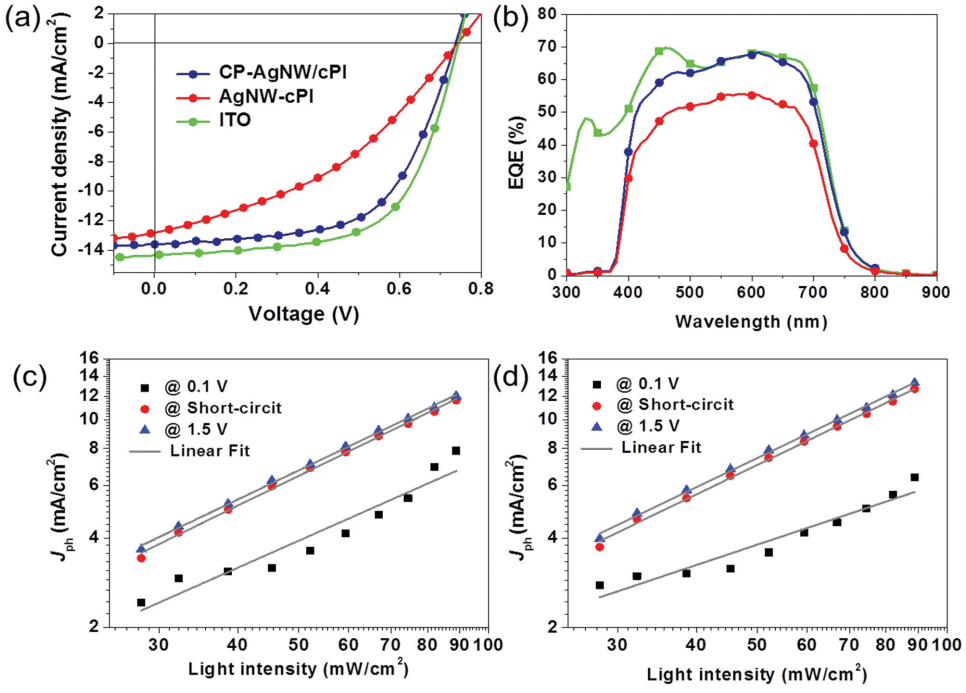

Figure 6. a) *J*–*V* characteristics and b) EQE spectra of various solar cell devices, as measured under a 88.8 mW cm^{-2} air mass and 1.5 global (AM 1.5G) illumination. Photocurrent as a function of light intensity at different effective voltages for a c) CP-AgNW/cPI- and d) AgNW/cPI-based solar cell.

Table 1. Characteristics of a P1 solar cell measured under a 88.8 mW/cm^2 air mass and 1.5 global (AM 1.5G) illumination.

Electrode		V_{oc} [V]	J_{sc} [mA cm^{-2}]	FF	PCE[a)] [%]
CP-AgNW/cPI	Best	0.740	13.61	0.600	6.81
	Ave.	0.739	13.71	0.592	6.75 ± 0.20
CP-AgNW	Best	0.742	12.82	0.393	4.21
	Ave.	0.742	12.62	0.388	4.09 ± 0.17
ITO	Best	0.741	14.38	0.619	7.43
	Ave.	0.740	14.01	0.600	7.01 ± 0.20

[a)]Average values of ten devices fabricated under identical conditions.

with AgNW-cPI based one. The nongeminate recombination of the solar cell devices was compared on the basis of the relation between their light intensity and photocurrent density, which can be modeled as a power law relationship $J \propto P^{\alpha}$, where P is the power generation rate and the deviation of α from unity is due to bimolecular recombination and the build-up of space charges in the active layer.[12] Figure 6c,d shows their photocurrent density ($J_{ph} = J_L - J_D$) as a function of light intensity at various effective voltages, where J_L and J_D are the current density under illumination and in the dark, respectively. The effective voltage is defined as $V_{eff} = V_0 - V_{appl}$, where V_0 is the compensation voltage at $J_{ph} = 0$ and V_{appl} is the applied voltage. It can be seen from this that there is a linear relationship between the logarithmic photocurrent density and light intensity for both polymer device types under short-circuit conditions, and at V_{eff} values of 0.1 and 1.5 V. Moreover, at $V_{eff} = 1.5$ V the slopes of both polymers are very similar to each other and approximately equal to 1, but at $V_{eff} = 0.1$ V the slope of CP-AgNW/cPI ($\alpha = 0.8$) increases relative to that of AgNW/cPI ($\alpha = 0.74$). This indicates that bimolecular recombination and space charge effects are reduced in the CP-AgNW/cPI based solar cell device.

Solar cell devices based on an ITO anode in place of the CP-AgNW/cPI electrode were also tested, which as shown in Figure 6a, resulted in a PCE of 7.44% with a J_{sc} of 14.38, a FF of 0.619, and V_{oc} of 0.741 V. This represents a 0.6% increase that can be attributed to the higher J_{sc} value, as the FF and V_{oc} values both show very little change. The difference in the photocurrent can be explained by the external quantum efficiency spectra of the device, in that there was no absorption loss below 350 nm in the CP-AgNW/cPI-based device. In addition, there was no observable absorption gain created at 400–450 nm by the TiO_2 optical spacer that was intended to spatially redistribute the light intensity within the device.[13] Nevertheless, the external quantum efficiency (EQE) spectra of the CP-AgNW/cPI- and ITO-based solar cell devices are very similar within the 500–800 nm wavelength range. The J_{sc} of the ITO-based device was calculated by integrating the EQE data with the AM1.5G solar spectrum (14.63 mA cm^{-2}) and found to be 1.23 mA cm^{-2} higher than the 13.40 mA cm^{-2} of the CP-AgNW/cPI-based device, a difference that is comparable to the difference in J_{sc} evident in their respective I–V curves. On the basis of this, it is argued that the performance of a CP-AgNW/cPI-based solar cell device is comparable to conventional ITO-based devices.

To confirm the excellent performance of the CP-AgNW/cPI electrode it was used to fabricate a solar cell device based on three different polymers, the performance of which is compared against an ITO-based device in the I–V curves in **Figure 7** and cell parameters in **Table 2**. It is apparent from this that all of solar cells based on a CP-AgNW/cPI electrode exhibited comparable performance to using an ITO film, with the flexible solar cell designated as P2 achieving a higher PCE (7.42%) than that of P1 (6.81%) due to its higher V_{oc} of 0.786 V. Such performance is comparable to the 7.67% PCE of the ITO-based device, and to the best of our knowledge, is the highest efficiency that has been achieved with an organic solar cell on a flexible plastic substrate. The P3 solar cell device showed slightly higher performance again due to its improved FF value, which is considered to result from its bulk heterojunction film having a more suitable surface morphology. Meanwhile, we performed photovoltaic measurements with best performance solar cells (P1 and P2 solar cells) under 1 sun condition (100 mW cm^{-2} air mass, 1.5 global (AM 1.5G) illumination) in air. The solar cell results are summarized in Table S1 (Supporting Information) and the corresponding J–V curves and EQE spectra are shown in Figure S14 (Supporting Information). P1 and P2 achieved PCEs up to 6.80% and 7.37%, respectively, using the CP-AgNW/cPI electrode. The photovoltaic performances of P1 and P2 solar cells tested under 1 sun in air are comparable to those obtained under 0.888 sun and N_2 in Table 1 and 2. It is believed that the developed solar cell devices consistently show good performances regardless of sun intensities and furthermore, they have relatively good air stabilities

Given that the primary goal of using a flexible electrode in organic electronic devices is to allow highly reliable optoelectronic performance under conditions of continuous mechanical deformation, mechanical stability tests were carried out on all of the solar cell devices fabricated as part of this study. Figure 7c shows the change in J_{sc}, FF, V_{oc}, and PCE that was observed in a CP-AgNW/cPI-based device after 1000 cycles of convex bending to a radius of 1, 3, or 5 mm, revealing very little degradation in the sense that V_{oc} remains almost the same, while FF is only reduced by 3%. The J_{sc} values, on the other hand, do show a more significant decrease of 5%–8%, but 90%–95% of the initial PCE is still maintained even at a bend radius of 1 mm. More importantly, when folded to a bending radius of ≈40 μm (equivalent to a tensile strain of 25%), the CP-AgNW/cPI-based devices still maintain an excellent mechanical durability with an average PCE reduction of ≈5% (Figure 7d). As far as we know, this is the smallest bending radius that has been achieved in an organic solar cell device without a far more substantial degradation in performance. What is more, even when the bending strain was increased to 50%, the solar cell still achieved an averaged PCE that was within 85% of its initial value. The decrease in PCE was possibly due to the cracks and buckles formed on the surface of Al layer as shown in Figure S15 (Supporting Information). It is necessary to be noted that the strain of 50% is much larger than the maximum elongation of pure Al that is 20%–30%. Nevertheless the results obtained here clearly demonstrate that flexible organic solar cell devices employing a CP-AgNW/cPI electrode can simultaneously provide excellent mechanical stability and a high photovoltaic performance that is comparable with ITO-based solar cell devices.

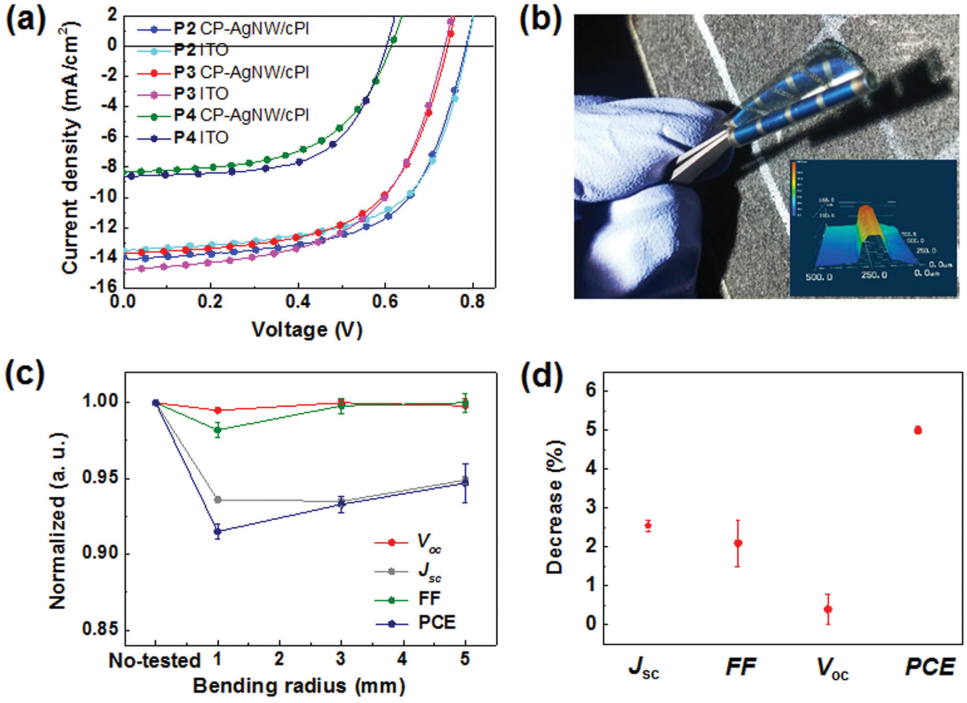

Figure 7. Measured performance of P2, P3, and P4 solar cells: a) *J–V* characteristics of solar cells prepared from CP-AgNW/cPI or ITO, b) photograph showing the flexibility of the device (inset shows a 3D profile of a sample bent to a radius of 70 μm), c) measured V_{oc}, J_{sc}, FF, and PCE of the solar cells as a function of bending radius after 1000 tension bending cycles (normalized to the initial value), d) change in the photovoltaic parameters of the solar cells after bending to a radius of 40 μm.

3. Conclusion

A highly flexible CP-AgNW composite electrode fully embedded in cPI has been successfully created through a solution-based inverted layer-by-layer process, and demonstrated to be both highly conductive and transparent. This composite electrode is based on a consecutively stacked AgNW network layer and a thin layer of conductive polymer, both of which are then overlayed with cPI. Thanks to the exceptionally good compatibility of the materials, the fabricated electrode has shown extreme flexibility, large conductive pathways, and uniform surface with a low roughness. Furthermore, the excellent mechanical stability of this electrode results in only a very small increase (<10%) in resistance when bent to a radius of 40 μm radius. A polymer solar cell based on this composite electrode therefore offers a very stable performance, with a PCE loss of no more than 5% when folded at a radius of 40 μm, with a maximum PCE of 7.42% being achievable. As this inverted layer-by-layer process used is easily scalable and highly reliable, it is believed that CP-AgNW/cPI electrodes have the potential to replace conventional sputtered transparent metal oxide materials such as ITO. The developed method is thought to be a good example which solved major challenges in metal nanowire-based transparent flexible electrode and the approaches demonstrated in this study is expected to be a guideline for fabrication of foldable electronic devices.

Table 2. Characteristics of polymer solar cells, as measured under a 88.8 mW cm^{-2} air mass and 1.5 global (AM 1.5G) illumination.

Polymer	Electrode		V_{oc} [V]	J_{sc} [mA cm^{-2}]	FF	PCE[a)] [%]
P2	CP-AgNW/cPI	Best	0.786	13.54	0.619	7.42
		Ave.	0.782	13.39	0.623	7.35 ± 0.21
	ITO	Best	0.784	13.95	0.623	7.67
		Ave.	0.782	13.87	0.616	7.52 ± 0.18
P3	CP-AgNW/cPI	Best	0.736	11.94	0.624	6.17
		Ave.	0.733	11.80	0.618	6.02 ± 0.14
	ITO	Best	0.730	12.61	0.583	6.04
		Ave.	0.730	12.58	0.577	5.97 ± 0.15
P4	CP-AgNW/cPI	Best	0.612	8.33	0.556	3.19
		Ave.	0.611	7.97	0.540	2.96 ± 0.16
	ITO	Best	0.602	8.63	0.610	3.57
		Ave.	0.604	8.56	0.605	3.52 ± 0.14

[a)]Average values of ten devices fabricated under identical conditions.

4. Experimental Section

Fabrication of CP-AgNW/cPI Electrode: The inverted layer-by-layer processing procedure used for the fabrication of the CP-AgNW/cPI transparent electrode is schematically illustrated in Figure 1a. In this, a glass substrate was first prepared by cleaning it with detergent, de-ionized water, acetone, and isopropanol, then onto this substrate was spin-coated a blend solution of neutral poly(3,4-ethylenedioxythiophene):-polystyrene sulfonate (PEDOT:PSS, DT-PEDOT-CDT-NT, Dittotechnology Ltd., Korea) with an epoxy based binding material by varying the rotation speed. The resulting film was annealed at 120 °C for 30 min, and then the PEDOT:PSS coated glass was placed on a Mayer rod apparatus. Several

drops (0.5 mL) of a nanowire solution (Nanopyxis Ltd., Korea) were then deposited onto the glass, and a Mayer rod #8 (R.D. Specialties, Inc., USA) was immediately rolled over them to evenly spread the nanowire solution over the PEDOT:PSS surface. This solution was then carefully dried under infrared illumination for 10 min. The stacked AgNW and PEDOT:PSS layers were etched by a dilute acidic solution (Chromium Etchant, Sigma-Aldrich), and then a colorless polyimide (cPI) varnish (Kolon, Korea) was spin-coated onto the cleaned glass and cured at 200 °C for 1 h. The thickness of this film could be precisely controlled by varying the spinning velocity, and so a thickness of 20 μm was selected to provide a suitable balance of flexibility and good reliability. Once the film was formed on the composite electrode, the sample was soaked in water to help safely peel the film from the supporting glass through hygroscopic swelling of the PEDOT:PSS layer and cPI film.

Measurement of the Composite Electrode: Scanning electron microscopy (SEM, JEOL Ltd., JSM6700F, Japan) was used to investigate the microstructure of the AgNW networks. Their optical transmittance and haziness were measured using a UV–visible spectrophotometer (Jasco, V-560, Japan). The sheet resistance was measured by a noncontact measurement system (Napson Corporation, EC-80P, Japan). The surface roughness was measured by atomic force microscopy (AFM, Park Systems, XE-100TM, USA), and a cross-section of each sample was prepared by a focused ion beam (FIB, JEOL Ltd., JIB-4601F, Japan) system. The mechanical stability of the CP-AgNW/cPI film after being peeled from the glass supporter was evaluated by two different methods. The first of these was to evaluate the actual foldability of the films with small bending radii from 160 to 40 μm, in which the sheet resistance measured before and after folding was used as an indicator of the folding endurance. An automatic bend testing machine (Toyoseiki Ltd., MIT-DA, Japan) was used to measure the long-term reliability under repeated bending cycles, with this particular device causing the electrodes to alternately experience outward bending (tensile stress) and inward bending (compressive stress) to a bending radius of 0.5 mm (≈2% tensile and compressive strain) until the point of cyclic fatigue failure. The electrodes were bent at a cycle rate of 1 Hz, and their resistance was measured during both the inward and outward bending cycles. A more detailed description of this testing method is provided in the Supporting Information.

Solar Cell Device Fabrication and Measurement: For fabrication of the solar cell devices, the peeled CP-AgNW/cPI film was made to adhere upside down to another glass by a gel-based adhesive film (Gel-Pack, Ltd., DGL-60-X4, USA). All of the organic solar cell devices used were fabricated with a normal device structure of CP-AgNW/cPI (or ITO)/hole transporting material/polymer:$PC_{71}BM$/TiO_2/Al. For this, ITO glass substrates were first cleaned in acetone, ethanol, and isopropanol for 10 min under ultrasonication, and then dried in a vacuum oven. The ITO substrates were then further treated with ultraviolet ozone for 20 min. In this study, PEDOT:PSS (Baytron P VP AI4083) was used as a hole transporting material, and this was spin-coated onto the precleaned electrode surface to form a 25–30 nm PEDOT:PSS layer. The films were then dried in a vacuum oven at 110 °C for 20 min. Next, a solution of each polymer:$PC_{71}BM$ blend was prepared by dissolving a mixture of the polymer to be tested and $PC_{71}BM$ in chlorobenzene with 3 vol% of 1,8-diiodooctane (DIO). The optimized ratios for these blend solutions were 1:1.5 wt/wt (25 mg mL^{-1}) for P1, P2, and P3 and 1:0.6 wt/wt (19.2 mg mL^{-1}) for P4. Each polymer:$PC_{71}BM$ blend solution was spin-coated onto a CP-AgNW/cPI (or ITO)/PEDOT:PSS substrate to form an active layer of ≈100 nm in thickness. To provide an interlayer, TiO_2 nanoparticles dispersed in ethanol were spin-coated on the top of the active layer. After transferring the resulting films into a vacuum chamber, a 100 nm thick Al layer was thermally evaporated through a shadow mask at a base pressure of 2×10^{-6} Torr to give a deposition rate of 5 Å s^{-1}. The active area was defined by the area of the top metal electrode (0.15 cm^2). The current density versus voltage (*J*–*V*) characteristics of the prepared organic solar cell devices were recorded under a N_2 atmosphere with a Keithley model 2400 source measuring unit. A class-A solar simulator with a xenon lamp (Newport 69907, beam size 2×2 inch) equipped with an AM 1.5 G filter was used as a light source, the intensity of which was adjusted to AM 1.5 G, 0.888 sun light intensity (88.8 mW cm^{-2}) using a NREL-calibrated Si solar cell. EQE was measured as a function of wavelength from 300 to 900 nm on incident photon-to-current conversion equipment (Mcscience). Calibration was performed using a NIST-calibrated G425 silicon photodiode equipped with a KG-5 filter as a standard.

Supporting Information

Supporting Information is available from the Wiley Online Library or from the author.

Acknowledgements

Y.K. and T.I.R. contributed equally to this work. This work was supported by the Global Frontier R&D Program of the Center for Multiscale Energy System funded by the National Research Foundation of the Ministry of Science (No.2N39300), and the Technology Innovation Program (10042412) funded by the Ministry of Trade, Industry & Energy, Korea. Support was also provided by the Korea Institute of Science and Technology (KIST) under Project Nos. 2V034000 and 2E25392, and the new and Renewable Energy Progam of the Korea Institute of Energy Technology Evaluation and Planning (KETEP) grant funded by the Korea Government Ministry of Trade, Industry & Energy (MTIE) (20113030010030).

Received: March 17, 2015
Revised: May 19, 2015
Published online: June 18, 2015

[1] a) D. R. Cairns, R. P. Witte, D. K. Sparacin, S. M. Sachsman, D. C. Paine, G. P. Crawford, R. R. Newton, *Appl. Phys. Lett.* **2000**, *76*, 1425; b) Z. Chen, B. Cotterell, W. Wang, E. Guenther, S. A. Chua, *Thin Solid Films* **2001**, *394*, 202; c) S. K. Park, J. I. Han, D. G. Moon, W. K. Kim, *Jpn. J. Appl. Phys.* **2003**, *42*, 623.

[2] N. Zhou, D. B. Buchholz, G. Zhu, X. Yu, H. Lin, A. Facchetti, T. J. Marks, R. P. H. Chang, *Adv. Mater.* **2014**, *26*, 1098.

[3] a) D. S. Hecht, L. Hu, G. Irvin, *Adv. Mater.* **2011**, *23*, 1482; b) Y. H. Kim, C. Sachse, M. L. Machala, C. May, L. Müller-Meskamp, K. Leo, *Adv. Funct. Mater.* **2011**, *21*, 1076; c) S.-I. Na, S.-S. Kim, J. Jo, D.-Y. Kim, *Adv. Mater.* **2008**, *20*, 4061.

[4] a) K. S. Novoselov, A. K. Geim, S. V. Morozov, D. Jiang, M. I. Katsnelson, I. V. Grigorieva, S. V. Dubonos, A. A. Firsov, *Nature* **2005**, *438*, 197; b) L. Gomez De Arco, Y. Zhang, C. W. Schlenker, K. Ryu, M. E. Thompson, C. Zhou, *ACS Nano* **2010**, *4*, 2865; c) T.-H. Han, Y. Lee, M.-R. Choi, S.-H. Woo, S.-H. Bae, B. H. Hong, J.-H. Ahn, T.-W. Lee, *Nat. Photonics* **2012**, *6*, 105; d) S. Iijima, T. Ichihashi, *Nature* **1993**, *363*, 603; e) K. S. Kim, Y. Zhao, H. Jang, S. Y. Lee, J. M. Kim, K. S. Kim, J.-H. Ahn, P. Kim, J.-Y. Choi, B. H. Hong, *Nature* **2009**, *457*, 706; e) T. Y. Kim, S. W. Kwon, S. J. Park, D. H. Yoon, K. S. Suh, W. S. Yang, *Adv. Mater.* **2011**, *23*, 2734.

[5] a) Z. Yin, S. Sun, T. Salim, S. Wu, X. Huang, Q. He, Y. M. Lam, H. Zhang, *ACS Nano* **2010**, *4*, 5263; b) M. Zhang, S. Fang, A. A. Zakhidov, S. B. Lee, A. E. Aliev, C. D. Williams, K. R. Atkinson, R. H. Baughman, *Science* **2005**, *309*, 1215; c) B. Dan, G. C. Irvin, M. Pasquali, *ACS Nano* **2009**, *3*, 835.

[6] a) M. Fahland, T. Vogt, W. Schoenberger, N. Schiller, *Thin Solid Films* **2008**, *516*, 5777; b) M.-G. Kang, M.-S. Kim, J. Kim, L. J. Guo, *Adv. Mater.* **2008**, *20*, 4408; c) B. O'Connor, C. Haughn, K.-H. An, K. P. Pipe, M. Shtein, *Appl. Phys. Lett.* **2008**, *93*, 223304; d) R. B. Pode, C. J. Lee, D. G. Moon, J. I. Han, *Appl. Phys. Lett.* **2004**, *84*, 4614; e) P. B. Catrysse, S. Fan, *Nano Lett.* **2010**, *10*, 2944; e) S. Liu, J. Yue, A. Gedanken, *Adv. Mater.* **2001**, *13*, 656;

f) Y. Sun, B. Gates, B. Mayers, Y. Xia, *Nano Lett.* **2002**, *2*, 165; g) Y. Sun, Y. Yin, B. T. Mayers, T. Herricks, Y. Xia, *Chem. Mater.* **2002**, *14*, 4736; h) D. Azulai, T. Belenkova, H. Gilon, Z. Barkay, G. Markovich, *Nano Lett.* **2009**, *9*, 4246; i) S. De, T. M. Higgins, P. E. Lyons, E. M. Doherty, P. N. Nirmalraj, W. J. Blau, J. J. Boland, J. N. Coleman, *ACS Nano* **2009**, *3*, 1767.

[7] L. Hu, H. S. Kim, J. Lee, P. Peumans, Y. Cui, *ACS Nano* **2010**, *4*, 2955.

[8] a) L. Li, Z. Yu, W. Hu, C. Chang, Q. Chen, Q. Pei, *Adv. Mater.* **2011**, *23*, 5563; b) W. Gaynor, S. Hofmann, M. G. Christoforo, C. Sachse, S. Mehra, A. Salleo, M. D. McGehee, M. C. Gather, B. Lüssem, L. Müller-Meskamp, P. Peumans, K. Leo, *Adv. Mater.* **2013**, *25*, 4006; c) J. Liang, L. Li, X. Niu, Z. Yu, Q. Pei, *Nat. Photonics* **2013**, *7*, 817.

[9] J.-A. Jeong, H.-K. Kim, *Appl. Phys. Lett.* **2014**, *104*, 071906.

[10] a) A. Kim, Y. Won, K. Woo, S. Jeong, J. Moon, *Adv. Funct. Mater.* **2014**, *24*, 2462; b) M.-S. Lee, K. Lee, S.-Y. Kim, H. Lee, J. Park, K.-H. Choi, H.-K. Kim, D.-G. Kim, D.-Y. Lee, J.-U. Nam, S. Park, *Nano Lett.* **2013**, *13*, 2814; c) L. Li, J. Liang, S.-Y. Chou, X. Zhu, X. Niu, Z. Yu, Q. Pei, *Sci. Rep.* **2014**, *4*, 4307; d) K. Zilberberg, F. Gasse, R. Pagui, A. Polywka, A. Behrendt, S. Trost, R. Heiderhoff, P. Görrn, T. Riedl, *Adv. Funct. Mater.* **2014**, *24*, 1671; e) T. Ito, S. Okazaki, *Nature* **2000**, *406*, 1027.

[11] K.-W. Seo, J.-H. Lee, H.-J. Kim, H.-K. Kim, S.-I. Na, *Appl. Phys. Lett.* **2014**, *105*, 031911.

[12] a) A. Moulé, K. Meerholz, *Appl. Phys. B* **2008**, *92*, 209; b) L. J. A. Koster, V. D. Mihailetchi, H. Xie, P. W. M. Blom, *App. Phys. Lett.* **2005**, *87*, 203502; c) S. R. Cowan, A. Roy, A. J. Heeger, *Phys. Rev. B* **2010**, *82*, 245207.

[13] J. Y. Kim, S. H. Kim, H. H. Lee, K. H. Lee, W. L. Ma, X. Bong, A. J. Heeger, *Adv. Mater.* **2006**, *18*, 572.